PAPER

Magneto-optical and thermal characteristics of magnetite nanoparticle-embedded DNA and CTMA-DNA thin films

View the article online for updates and enhancements.

Magneto-optical and thermal characteristics of magnetite nanoparticle-embedded DNA and CTMA-DNA thin films

Mallikarjuna Reddy Kesama[1] , **Byung Kil Yun**[2], **Taewoo Ha**[3],
Sreekantha Reddy Dugasani[1] , **Junyoung Son**[1], **Jae Hoon Kim**[3,4],
Joung Hoon Jung[2,4] and **Sung Ha Park**[1,4]

[1] Department of Physics and Sungkyunkwan Advanced Institute of Nanotechnology (SAINT),
Sungkyunkwan University, Suwon 16419, Republic of Korea
[2] Department of Physics, Inha University, Incheon 22212, Republic of Korea
[3] Department of Physics, Yonsei University, Seoul 03722, Republic of Korea

E-mail: super@yonsei.ac.kr, jhjung@inha.ac.kr and sunghapark@skku.edu

Abstract

Recently, DNA molecules embedded with magnetite (Fe_3O_4) nanoparticles (MNPs) drew much attention for their wide range of potential usage. With specific intrinsic properties such as low optical loss, high transparency, large band gap, high dielectric constant, potential for molecular recognition, and their biodegradable nature, the DNA molecule can serve as an effective template or scaffold for various functionalized nanomaterials. With the aid of cetyltrimethylammonium (CTMA) surfactant, DNA can be used in organic-based applications as well as water-based ones. Here, DNA and CTMA-DNA thin films with various concentrations of MNPs fabricated by the drop-casting method have been characterized by optical absorption, refractive index, Raman, and cathodoluminescence measurements to understand the binding, dispersion, chemical identification/functional modes, and energy transfer mechanisms, respectively. In addition, magnetization was measured as a function of either applied magnetic field or temperature in field cooling and zero field cooling. Saturation magnetization and blocking temperature demonstrate the importance of MNPs in DNA and CTMA-DNA thin films. Finally, we examine the thermal stabilities of MNP-embedded DNA and CTMA-DNA thin films through thermogravimetric analysis, derivative thermogravimetry, and differential thermal analysis. The unique optical, magnetic, and thermal characteristics of MNP-embedded DNA and CTMA-DNA thin films will prove important to fields such as spintronics, biomedicine, and function-embedded sensors and devices.

Supplementary material for this article is available online

(Some figures may appear in colour only in the online journal)

1. Introduction

Deoxyribonucleic acid (DNA), one of the most promising and ubiquitous host template biomaterials, has been processed from salmon fish roe and milt sacs. DNA obtained from salmon fish possesses its typical intrinsic features such as structural stability, low optical loss, and high transparency. Inherently biodegradable DNA interacts with a wide range of functional materials via molecular recognition which makes DNA a potential smart material for fabricating nanostructures

---

[4] Authors to whom any correspondence should be addressed.
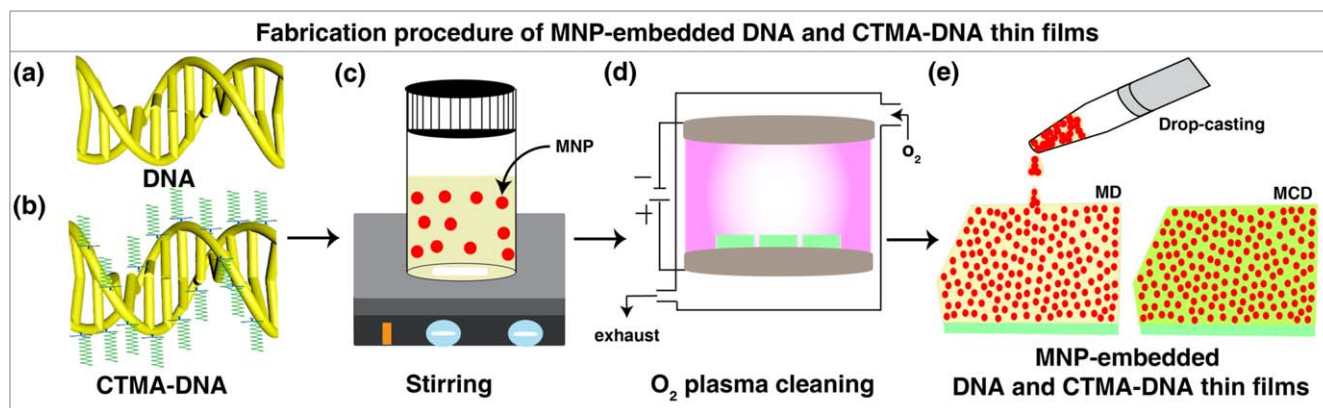
Figure 1. Fabrication procedure of DNA and cetyltrimethylammonium chloride functionalized DNA (CTMA-DNA) thin films embedded with magnetite (Fe_3O_4) nanoparticles (MNPs). (a)–(d) Schematics of DNA dissolved in aqueous solution, CTMA-DNA dissolved in 1-butanol, magnetic stirring to mix the MNPs in DNA solution, and O_2 plasma cleaning to remove contaminants from the substrates. (e) Fabrication of MNP-embedded DNA (labeled as MD) and CTMA-DNA (labeled as MCD) thin films constructed by drop-casting method.

[1]. Although DNA is typically soluble in aqueous solution, simple modification with cetyltrimethylammonium (CTMA) surfactant makes it soluble in organic solvents as well, improving the range of applications. DNA (dissolved in water) and CTMA-DNA (dissolved in 1-Butanol) are poised to become viable biopolymer materials with significant potential use in various physical, chemical, and biological devices and sensors such as FETs, OLEDs, solar cells, optical switches, and gas sensors [2–5]. DNA functionality can be easily enhanced by incorporating specific nanomaterials such as ions, carbon-based materials, nanoparticles, quantum dots, fluorescent dyes, conductive polymers, drug molecules, and proteins [6–12].

Because of the relatively low toxicity and lower oxidation ability, magnetic magnetite (Fe_3O_4) nanoparticles (MNPs) may be useful in *in vivo* medical diagnostics as well as oxygen rich environments. In fact, MNPs are already commonly used for particle synthesis and catalytic activity to aid the degradation of organic materials. The large magnetic moment and saturation magnetization of MNPs may be useful in high-density magnetic recording media, magnetic imaging, magnetic fluids, single magnetic domain devices, and spin valves [8, 13, 14].

Given relatively large surface-to-volume ratios, MNPs tend to aggregate in solutions due to entropic force produced via depletion zone reduction. Selecting a proper surfactant is critical to obtain stable and uniformly dispersed MNPs in either aqueous or organic solvents [15]. Among numerous surfactants, DNA and CTMA-DNA molecules have won approval in overcoming the agglomeration of MNPs by reducing the entropy via their non-covalent interaction affinity for MNPs. Efficient dispersion of MNPs without modification in the medium is important to enhance functionality without degrading physical properties.

Stable magnetite MNPs have been used for innumerable *in vivo* biomedical applications to improve diagnostics and therapeutics due to their inimitable magnetic performance under an applied magnetic field [16, 17]. The Neel and Brownian relaxation of MNPs under the alternative magnetic field contribute to generate thermal energy which has been used in hyperthermia and chemotherapy [18]. In addition to biomedical applications, MNPs have been used in physical and chemical devices and sensors [19–21].

Although the fabrication and characteristics of metallic and semiconducting nanoparticle-embedded DNA have been studied intensively, DNA and CTMA-DNA with MNPs are seldom discussed because of fabrication and optimization limits in both aqueous and organic solvents. In this paper, we introduce efficient fabrication methodology for DNA and CTMA-DNA thin films embedded with MNPs. We characterize the thin films by UV–vis absorption, refractive index and extinction coefficient, Raman spectroscopy, cathodoluminescence (CL), and applied magnetic field-dependent and temperature-dependent magnetizations. Thermal properties (i.e., thermogravimetric analysis (TGA), derivative thermogravimetry (DTG), and differential thermal analysis (DTA)) of MNP-embedded DNA (MD) and CTMA-DNA (MCD) thin films are discussed.

2. Experimental section

2.1. Synthesis of CTMA-modified DNA molecules

DNA fiber (GEM Corporation, Shiga, Japan) extracted from salmon by enzyme isolation process is water soluble but insoluble in organic solvents. To disperse in organic solvents, the DNA was modified by an ion-exchange reaction process through addition of cetyltrimethylammonium (CTMA) cationic surfactant (Sigma-Aldrich, USA). The resulting CTMA-modified DNA (CTMA-DNA) is soluble in organic solvent. The stepwise procedure for CTMA-DNA preparation is given here. 3 g of DNA fiber was dissolved in 1 l of deionized (DI) water with magnetic stirring (800 rpm) at room temperature for 10 h. In a separate beaker containing 1 l of DI water, 6 ml of CTMA chloride solution was stirred (800 rpm) at room temperature for 2 h. The CTMA surfactant was then added to the DNA solution slowly through a syringe followed by 3 h of stirring (800 rpm). The CTMA surfactant-modified

DNA precipitate along with residual CTMA and NaCl was collected. Residual CTMA and NaCl were removed by filtration process. The filtered CTMA-DNA was dried overnight at around 50 °C to obtain CTMA-DNA powder. The CTMA-DNA powder thus prepared is ready for solvation in 1-butanol. (figures 1(a)–(c)).

2.2. O$_2$ plasma cleaning process

O$_2$ plasma cleaning is a simple and effective method to clean (remove organic contaminants) the substrate surface and modify (enhance hydrophilic characteristics) them. Operating parameters of O$_2$ plasma cleaner (CUTE CUTE-1MP/R, Gyeonggi, Korea) were as follows: base pressure of 5×10^{-2} Torr, process pressure of 7.5×10^{-1} Torr, power of 45 W, O$_2$ gas flow rate of 45 SCCM, and processing time of about 5 min (figure 1(d)).

2.3. Fabrication of pristine, MNP-embedded DNA and CTMA-DNA thin films

White DNA fiber extracted from salmon was purchased from GEM Corporation, Shiga, Japan. The 0.5 weight-percentage (wt%) DNA (CTMA-DNA) solution with various concentrations (0, 2, 5, 10, 50, and 100 mg) of MNPs of size 20–30 nm (3320DX, Skyspring Nanomaterials, Inc., USA) was obtained by dissolving 0.025 g of DNA (CTMA-DNA) in 5 ml of DI water (1-Butanol) solvent followed by stirring (1000 rpm) for 12 h at room temperature to attain a homogeneous DNA and MNP solution. MNP-embedded DNA (CTMA-DNA) thin films were prepared by drop-casting onto various substrates (fused silica for absorption and cathodoluminescence, silica for refractive index and extinction coefficient, and glass for Raman and magnetic measurements) pre-treated with O$_2$ plasma. Substrate size was 5 mm × 5 mm for all experiments except magnetic ones (3 mm × 3 mm). A drop volume of 20 μl of DNA (CTMA-DNA) solution was used for the larger substrates and 7.2 μl for the smaller ones. Thin films of roughly 1.5 μm thickness of MNP-embedded DNA (CTMA-DNA) were obtained (figures 1(a)–(e)). We also constructed free-standing DNA (CTMA-DNA) thin films with varying concentration of MNPs by pouring 20 ml of a mixture of DNA (CTMA-DNA) and MNP solution into a 2 inch petri dish followed by drying in a 45 °C oven for about 3 days. The dried thin films need to be gently peeled off the petri dish.

2.4. Absorbance

The spectrophotometer (Agilent Cary 5000, Varian, USA) was used to measure the optical absorption properties of DNA and CTMA-DNA thin films with varied quantities of MNPs in the wavelength range from 190 to 800 nm. (Figures 2 and S1(a) are available online at stacks.iop.org/NANO/29/465703/mmedia in online supplementary data (OSD).)

2.5. Refractive index and extinction coefficient

The refractive index (*n*) and extinction coefficient (*k*) were extracted from phase and amplitude of light passing through DNA (CTMA-DNA) thin films with various quantities of MNPs as measured by ellipsometer (GES-5, SOPRA, USA). The ellipsometer operated with parameters as follows: photon energy ranging from 1.5 (visible region) to 5 eV (UV) at an incidence angle of 75° and measuring time of 0.3 s at a fixed wavelength of 2 nm. (Figures 3, S1(b), and table S1 in OSD.)

2.6. Raman spectrum

A confocal Raman spectroscope (WITEC, alpha 300 R) with an excitation wavelength of 532 nm was used to collect Raman spectra of MNP-embedded DNA and CTMA-DNA thin films. (Figures 4, S1(c), and table S2 in OSD.)

2.7. Cathodoluminescence (CL)

CL study of the MNP-embedded DNA thin films was carried out using a Gatan Mono CL^{3+} probe spectrometer attached to a scanning electron microscope (SU-70, Hitachi, Japan). An accelerating voltage of 20 kV was applied to generate sufficient signal for high intensity luminescence from the sample with a working distance of ∼8 mm. (Figures 5 and S1(d) in OSD.)

2.8. Magnetic characteristics

Magnetic field (*H*)-dependent magnetic moment (*m*) properties were studied using a vibrating sample magnetometer (VSM, PPMS-9, Quantum Design, CA, USA). The substrate-held samples were placed in the VSM to measure *m* with respect to *H* (up to 10 kOe) at room temperature. In addition, DNA and CTMA-DNA thin films of fixed MNP quantity (100 mg) were measured for temperature (*T*)-dependent *m* (*T* range from 2 to 300 K) at fixed *H* (200 Oe) by VSM in two cooling modes; field-cooling (FC) and zero field-cooling (ZFC). In FC (ZFC) mode of operation, the sample was kept at a fixed *H* of 200 Oe (without *H*) while cooling from 300 to 2 K. Then, the *m* of the sample at a fixed *H* of 200 Oe was measured by increasing *T* for both FC and ZFC modes. (Figures 6, 7, S1(e), and table S3 in OSD.)

2.9. Thermal analysis

TGA, DTG, and DTA of free-standing DNA (CTMA-DNA) thin films with various quantities of MNPs were carried out by thermal analyzer (TG/DTA7300 Seiko instruments, Japan). Initial free-standing thin film sample weight was 9.2 mg. Weight loss and heat flow changes of the thin film were measured from room temperature to 600 °C with a constant heating rate of 10 °C min^{-1} in a nitrogen gas chamber. (Figures 8, S1(f), and S2 in OSD.)
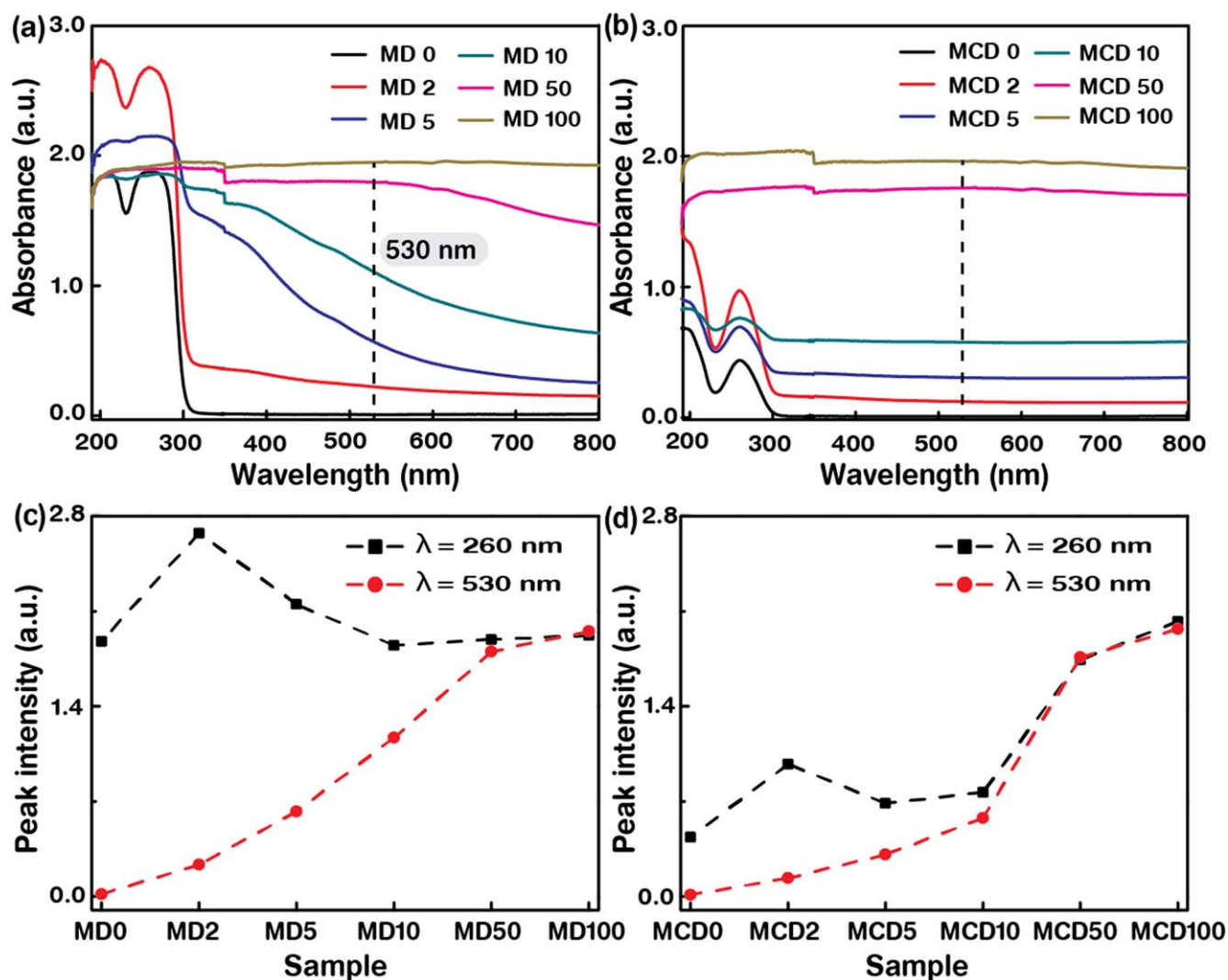
Figure 2. UV–vis absorption characteristics of MNP-embedded DNA (MD) and CTMA-DNA (MCD) thin films. (a) Optical absorption spectra of DNA thin films with various concentrations of MNPs [MNP] (0, 2, 5, 10, 50 and 100 mg labeled as MD 0, MD 2, MD 5, MD 10, MD 50 and MD 100, respectively). (b) Optical absorption spectra of CTMA-DNA thin films with various [MNP] as labeled previously. (c), (d) The absorption peak intensities as a function of [MNP] in MD and MCD thin films measured at fixed wavelengths of 260 (DNA) and 530 nm (MNPs).

3. Results and discussion

Figure 1 displays the schematic of fabrication and characterization procedures for DNA and CTMA-DNA thin films embedded with magnetite (Fe_3O_4) MNPs. Both homogeneous DNA in DI water and CTMA-DNA in 1-Butanol serve as structural templates and efficient surfactants for MNPs to minimize agglomeration and enhance optical, magnetic, and thermal characteristics. We prepared mixtures of DNA and CTMA-DNA with various concentrations of MNPs by dropcasting onto an O_2 plasma-treated substrate. The resulting MD and MCD thin films had a thickness of $\sim 1.5\,\mu$m (figures 1(a)–(e)).

Figure 2 shows UV–vis absorption characteristics of DNA and CTMA-DNA thin films with various concentrations of MNPs ([MNP]) at a fixed DNA concentration of 0.5 wt%. MD and MCD thin films were fabricated on a fused silica substrate to avoid background absorbance in the UV–vis

region. The DNA characteristic absorption peaks at $\sim$210 nm (due to sugar and phosphate groups where the electron transition referred to $n-\pi^*$ from HOMO to LUMO) and $\sim$260 nm (due to π conjugated electrons in the phenyl rings where the electron transition referred to $\pi-\pi^*$) were clearly visible in figures 2(a), (b) [22].

Absorption spectra of DNA and CTMA-DNA thin films were collected with varied [MNP]. In the range between 300 and 800 nm (representative wavelength of 530 nm marked as a dotted line), absorption increased with increasing [MNP] [23, 24]. Over this wavelength range, absorption increased roughly linearly along with increased [MNP] up to 10 mg quantity of MNP. At higher [MNP] (50 and 100 mg quantities), MD and MCD absorption peaks were suppressed. Here, the MNPs in DNA and CTMA-DNA thin films affect the absorption spectra not only by their electronic absorption but also through Rayleigh scattering. The red shifted absorption band edge transitions above 280 nm wavelength
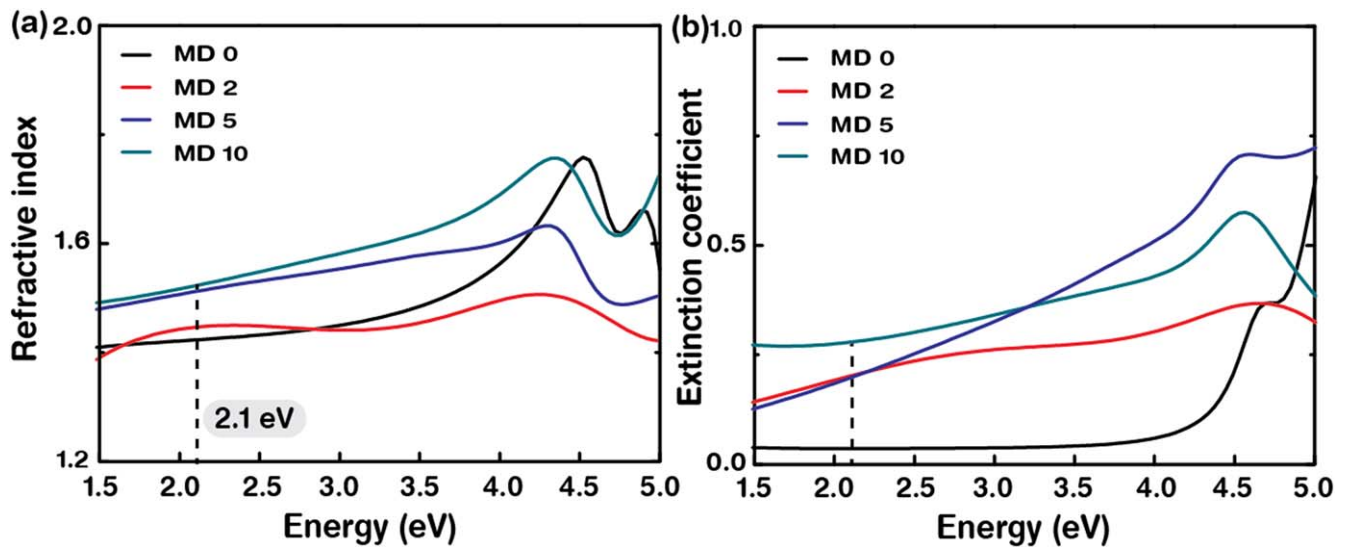
Figure 3. Refractive index and extinction coefficient characteristics of MNP-embedded DNA (MD) thin films. (a) Refractive indices of DNA thin films with various [MNP] as a function of photon energy. Photon energy of 2.1 eV marked as a dotted line in the graph corresponds to light of wavelength 589 nm in vacuum. (b) Extinction coefficients as a function of photon energy of DNA thin films with various [MNP].
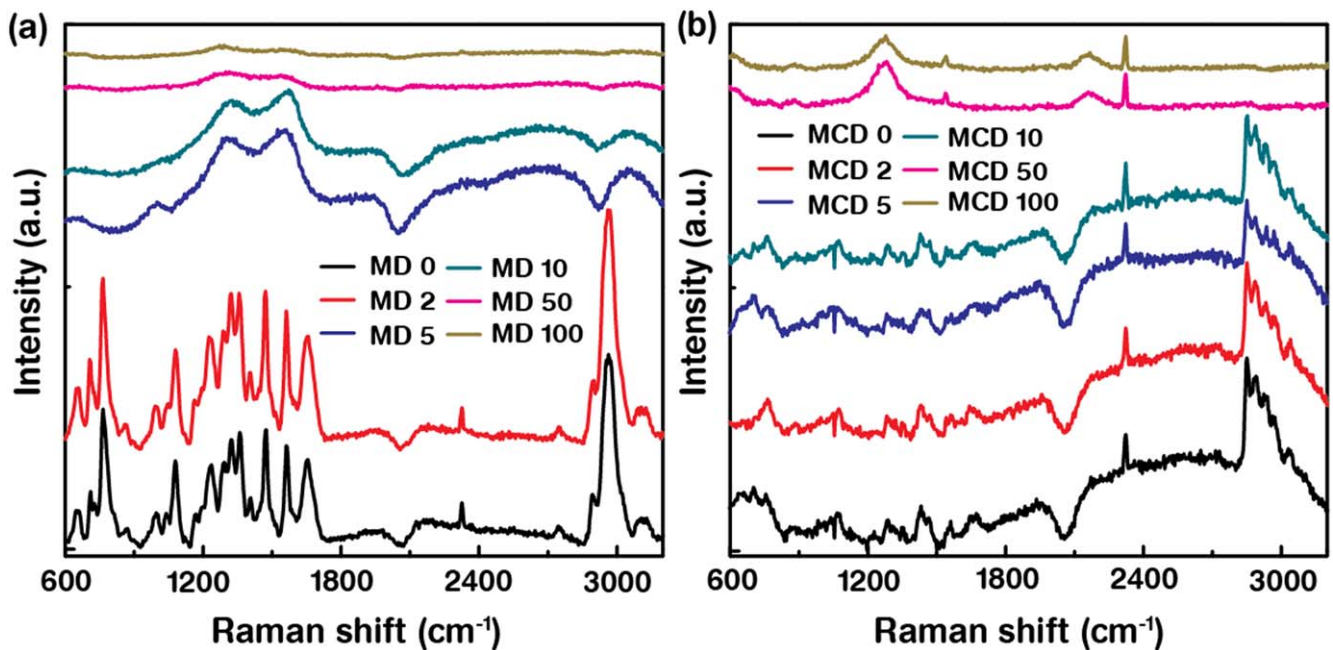
Figure 4. Raman spectra of MNP-embedded DNA (MD) and CTMA-DNA (MCD) thin films. Intensities of Raman spectra of DNA thin films with various [MNP] (i.e., MD 0, MD 2, MD 5, MD 10, MD 50, and MD 100) and CTMA-DNA thin films with various [MNP] as described previously. The Raman peaks of MD 0 and MCD 0 result from nucleobases, sugars, and phosphate backbones of DNA in the range of 600–1800 cm^{-1}, OH groups from the solvent show around 2950 cm^{-1}, and CTMA surfactant shows around 2850 cm^{-1}. Peak intensities are significantly influenced by the addition of MNPs.

occur due to non-covalent interactions between DNA (CTMA-DNA) and MNPs. In figures 2(c), (d), the absorption peak intensities of MD and MCD thin films are plotted as a function of [MNP] as measured at fixed wavelengths of 260 and 530 nm. Even though the DNA characteristic absorption peak position at 260 nm did not change much, peak intensities of MD showed relatively higher absorption than MCD due to differences in solvent characteristics such as viscosity and evaporation rate [25, 26].

Optical constants such as refractive index (*n*) and extinction coefficient (*k*) characteristic of MD thin films with various [MNP] were obtained by ellipsometer. For evaluating the *n* and *k*, we used DNA and CTMA-DNA thin films with relatively lower [MNP] in order to avoid the improper electronic transitions. Interactions of light passing through the MD thin films are well described by *n* (light retardation by the medium) and *k* (attenuation due to the absorption of light through the medium) as a function of photon energy from
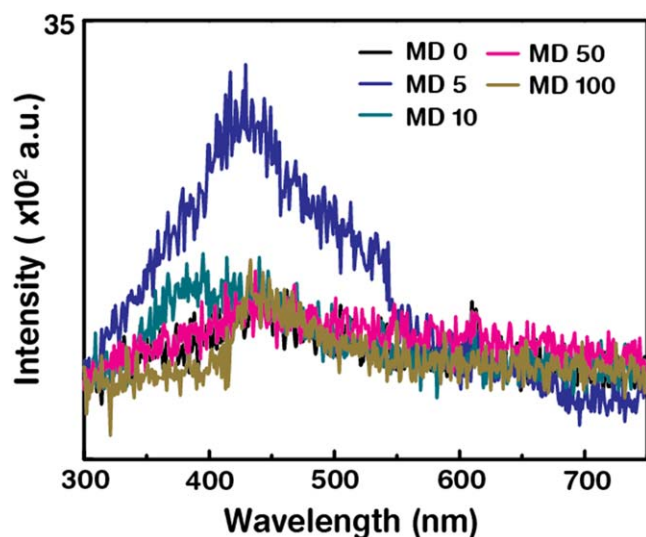
Figure 5. Cathodoluminescence (CL) studies of MNP-embedded DNA (MD) thin films with various [MNP] (i.e., MD 0, MD 5, MD 10, MD 50, and MD 100). Trace MD 5 was more intense than other traces.

1.5 to 5 eV. By obtaining the amplitude and phase of the light through the medium, we extract the complex permittivity ε, (which is correlated with polarizability, localized transitions, lattice vibration, atomic bonds, and molecular electronic transitions) followed by calculation of analytical parameters such as oscillator frequency, scattering rate, and plasma frequency through the interactions of MD thin films. Consequently, n and k are obtained from the relation of the real part ($\varepsilon_1 = n^2 - k^2$) and the imaginary part ($\varepsilon_2 = 2nk$) in ε ($=\varepsilon_1 + i\varepsilon_2$). Figure 3 displays n and k traces of MD thin films with various [MNP] as a function of photon energy. Roughly, the n and k values increase with increasing photon energy (normal dispersion). n and k peaks of MD thin films showed clear shifts from 4.75 eV to lower energy side (produced by pristine DNA thin films due to π electron excitation in the bases) influenced by [MNP] in the thin films. From the experimental data, we observe that the n and k values vary with the [MNP] in the DNA thin films. For instance, at fixed photon energy of 2.1 eV, n and k values increase with increasing [MNP] due to the interactions of the light with the different MNPs in the medium of MD thin films (numerical values of n and k are shown in table S1 in OSD). This could be due to homogeneity, molecule density, surface roughness, humidity, birefringence, or anisotropy in the MD thin films [22, 27–29].

Raman spectroscopic characteristics of MD and MCD thin films were collected and studied for chemical identification, effects of chemical bonding, and molecular structure in different solvents. The Raman vibrational spectrum of the molecule results in part from the masses of the atoms present, the strength of their chemical bonds, and their arrangement in the molecule. Therefore, different molecules have different vibrational Raman spectra. Raman spectra of MD and MCD thin films with various [MNP] are shown in figure 4. The Raman bands centered at around 660, 710, 765, 870, 990, 1080, 1230, 1285, 1325, 1360, 1400, 1470, 1565, 1655, and 2800–3100 cm^{-1} indicate different vibrational and stretching

modes of DNA and CTMA-DNA, and MNPs in water and 1-Butanol solvents. Raman shifts, and corresponding modes of DNA molecules are shown in table S2 in OSD.

The Raman bands can be classified into two regions, i.e., 600–1800 cm^{-1} from nucleobase, sugar, and phosphate backbone group interactions and 2800–3100 cm^{-1} for solvents and CTMA interactions. For instance, representative modes at 660, 765, 1080, and 1655 cm^{-1} are assigned respectively to ring breathing vibrational modes of guanine and thymine, symmetric stretching vibrational modes of PO_2^-, phosphodiester stretching vibrational modes, and the C=O stretching vibrational modes of thymine and cytosine. The Raman bands at 2890 and 2970 cm^{-1} are attributable to the stretching modes of water molecules in MD thin films and those at 2850, 2888, 2930, 2970, and 3037 cm^{-1} are stretching vibrations of CH_2 and CH_3 groups in the alkyl chains of CTMA in MCD thin films. Complete Raman shifts and corresponding modes of MD and MCD thin films are listed in table S2, OSD [30, 31]. The intensities of characteristic Raman peaks of MD and MCD thin films reduce with increasing [MNP] due to the high density of MNPs and Raman scattering [32–34]. In addition, we observed peak broadening at [MNP].

Figure 5 shows the CL behavior of MD thin films with various [MNP] to understand the energy transfer between the MNPs and DNA. An accelerating voltage of 20 kV (which minimized damage of the sample) was applied to generate sufficient signal for high luminescent intensity. The broad blue CL emission peaks of DNA thin film with MNPs were observed centered at around a wavelength of 420 nm. Fluorescent intensity was enhanced at a relatively low [MNP] in trace MD 5. Thereafter, the fluorescent intensity decreased as the [MNP] increased, which may be attributable to collision quenching at high [MNP]. At high [MNP], the MNP quenchers and DNA fluorophores are held closer together. Therefore, the energy absorbed by the fluorophore can be transferred easily to the MNPs. Eventually, the MNP-absorbed energy could disperse as heat causing decreased fluorescence [25, 35–37].

To understand magnetic behaviors such as magnetization (M) and saturation magnetization (M_S), the magnetic moment (m) as a function of an applied magnetic field (H) of MD and MCD thin films was measured by VSM. Here, m of bare glass was subtracted to remove the substrate effect. M can be obtained from m at a given sample volume (V) ($M = m/V$). Here, V of the thin film was $0.3 \times 0.3 \times (1.5 \times 10^{-4})$ cm^3. The graphs in figure 6 show M of MD and MCD thin films with various [MNP]. DNA and CTMA-DNA thin films (paramagnetic property) with MNPs (superparamagnetic property) could be used in various applications such as memory storage, low power consumption, and rapid information retrieval devices and sensors [38–41].

Figure 6 shows M–H curves and M_S characterized as a function of various [MNP] in DNA and CTMA-DNA thin films at a fixed T (300 K). The M increased monotonically with increasing [MNP] in the thin film along the H direction and reached close to the M_S. Due to superparamagnetic nature with nearly zero remnant magnetization (M at zero H) and
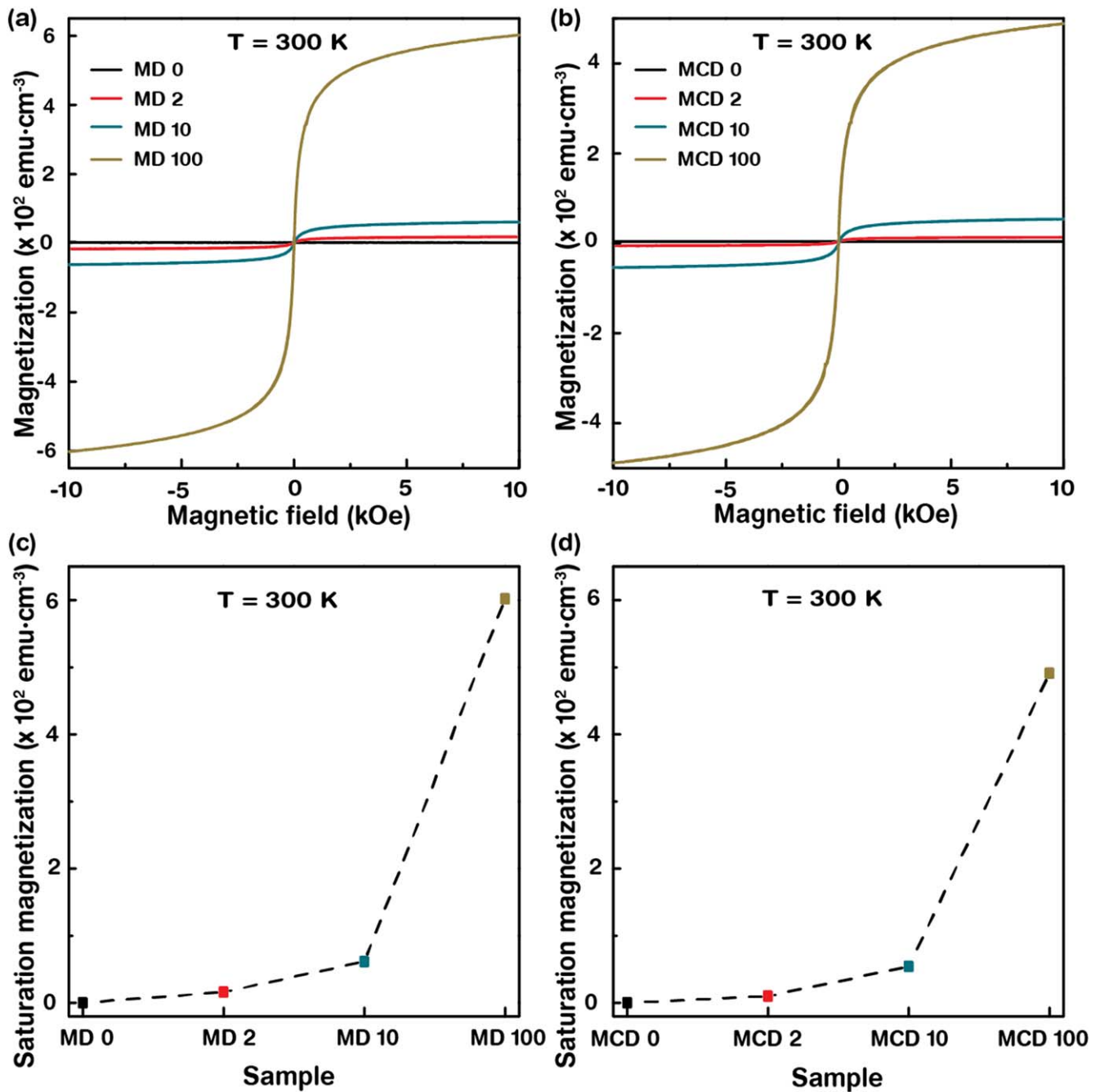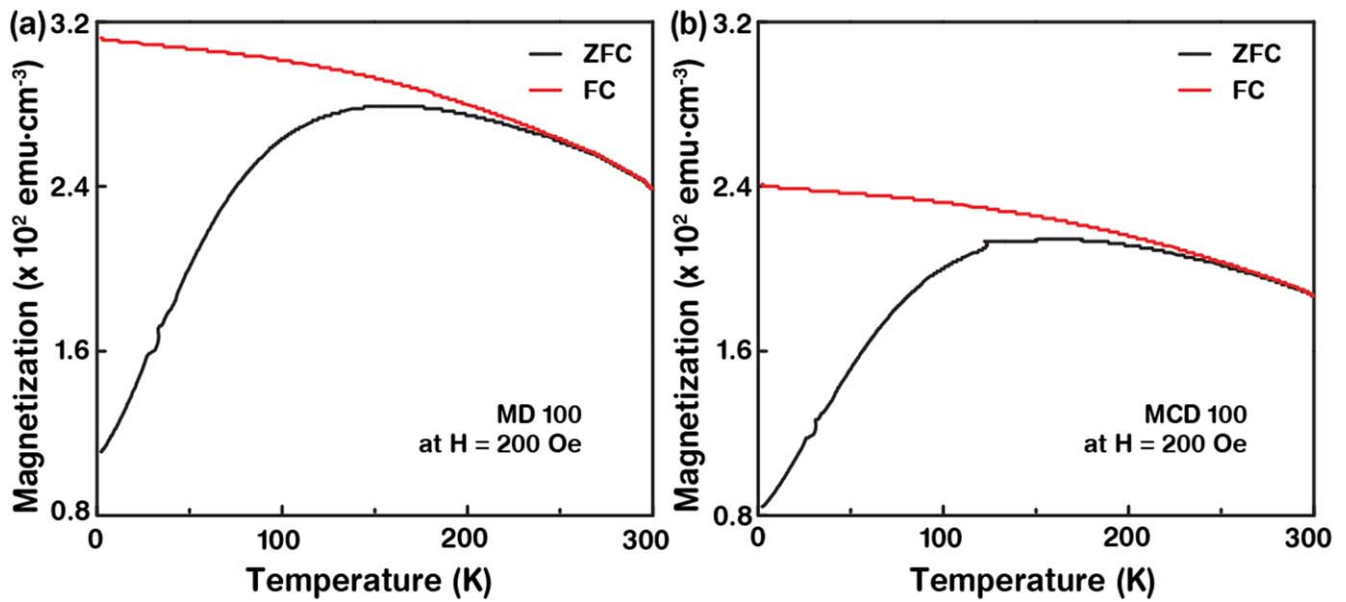
Figure 6. The magnetization (*M*) of MNP-embedded DNA (MD) and CTMA-DNA (MCD) thin films. (a), (b) *M* of DNA thin films with various [MNP] (MD 0, MD 2, MD 10, and MD 100) and CTMA-DNA thin films with similar reported [MNP] as a function of an applied magnetic field (*H*) measured at room temperature (300 K). (c), (d) Saturation magnetization of MD and MCD thin films obtained at *H* of 10 kOe.

coercivity (*H* at zero *M*) of MNPs, MD and MCD thin films reveal the dominant superparamagnetic behavior. Below the blocking temperature (*T_B* of ~150 K, magnetic anisotropy barrier), notable hysteresis in *M–H* curves can be seen which represents the ferromagnetic characteristics of MD and MCD thin films (data not shown). Because of differing solvent characteristics and the presence of CTMA causing reduction of the MNP dipole interaction, *M* of the MCD thin film (490 emu cm^{-3} at 10 kOe) measured less than *M* of the MD thin film (600 emu cm^{-3}) [42, 43]. The *M_S* obtained at *H* of

10 kOe of MD and MCD thin films are shown in figures 6(c), (d). The *M_S* increase with increasing [MNP], as expected.

T-dependent *M* of MD and MCD thin films was studied by a FC and a ZFC procedure to identify the phase transition of magnetism (*T_B*), MNPs distribution, and strength of interparticle interaction. In FC (ZFC) mode, the MD and MCD thin films were placed at a fixed *H* of 200 Oe (without *H*) during the course of cooling from 300 to 2 K. Then, *m* of the thin films at a fixed *H* of 200 Oe was measured by increasing *T* for both FC and ZFC modes.

Figure 7. Temperature-dependent magnetization (*T*–*M*) of MNP-embedded DNA (MD) and CTMA-DNA (MCD) thin films. (a), (b) *M* as a function of *T* (2–300 K) of MD 100 and MCD 100 thin films at a fixed *H* of 200 Oe under field cooling (FC) and zero field cooling (ZFC) modes. The magnetic phase transition to superparamagnetism and configuration of MNPs in DNA and CTMA-DNA thin films can be estimated.
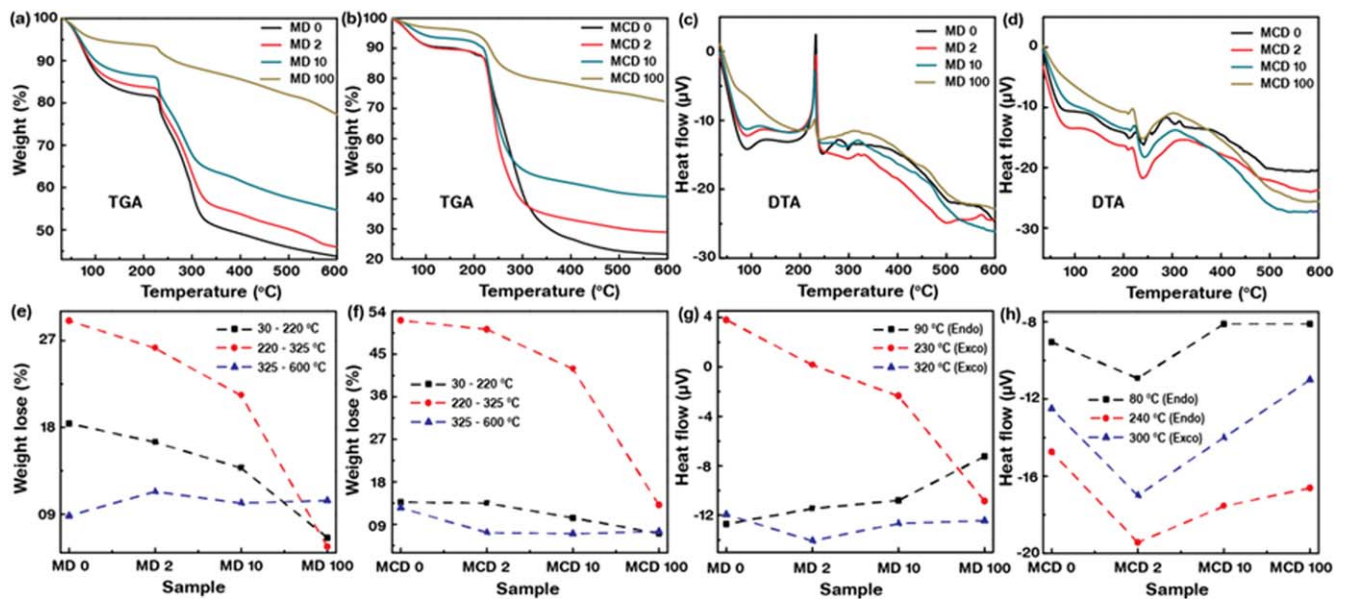
Figure 8. The thermogravimetry analysis (TGA) and differential thermal analysis (DTA) of MNP-embedded DNA (MD) and CTMA-DNA (MCD) thin films. (a), (b) Weight loss of DNA thin films with various [MNP] (i.e., MD 0, MD 2, MD 10, and MD 100) and CTMA-DNA thin films with reported [MNP] as a function of temperature. (c), (d) The DTA of DNA and CTMA-DNA thin films with various [MNP]. (e), (f) The weight loss of DNA and CTMA-DNA thin films with various [MNP] in three different temperature regions (30 °C–220 °C, 220 °C–325 °C, and 325 °C–600 °C). (g), (h) The endothermic and exothermic reactions at three characteristic temperatures of MD and MCD thin films obtained by differential thermal analysis.

Initially, *M* of the MD and MCD thin films was 0 at *H* of 0 Oe since *m* of individual MNPs were randomly oriented. With an external *H*, *m* of individual MNPs tended to orient along the direction of *H*. With increasing *T*, *M* gradually increases to the maximum *M* at T_B (ZFC curves in figure 7). At T_B, the magnetic transition of MD and MCD thin films from ferromagnetism to superparamagnetism is observed, indicating that the thermal energy above T_B overcame the

anisotropy barrier. In FC mode, *M* monotonically decreased as *T* increased. The difference in *M* ($=M_{ZFC} - M_{FC}$) at T_B was attributed to the existence of the magnetic anisotropy barrier. The branchement *T* (T_{Bra}) in the FC curve is defined as where M_{FC} equals to M_{ZFC} at T_B. In addition, a divergence of M_{ZFC} and M_{FC} curves from one another occurs at a certain *T* which was assigned as *T* of irreversibility (T_{irr}). Small temperature differences were observed between MD and MCD thin films.

Their T_B differs by 4 K, T_{Bra} by 10 K, and T_{irr} by 20 K, all of which originate from the different solvents. The comparison of T_B, T_{irr}, T_{Bra}, M_{ZFC} of MD and MCD thin films with 100 mg quantity of [MNP] is shown in table S3 in OSD. Relatively low M and T_{irr} of pristine MNPs compare to MD and MCD thin films reported in the literature [42, 44]. Differences may be due to the aggregation of MNPs. As a template and surfactant, DNA provided a stable and uniform dispersal medium for MNPs.

TGA, DTG, and DTA of free-standing DNA (CTMA-DNA) thin films with various [MNP] were carried out using a thermal analyzer. Free-standing MD and MCD thin films were constructed by pouring 20 ml of mixture of DNA (CTMA-DNA) and MNP solution into a petri dish followed by incubation at 45 °C for 3 days. Through thermal analysis, we studied physical changes (i.e., phase transformation and structural changes) and chemical characteristics (i.e., decomposition and chemical reactions) of materials influenced by T.

Figure 8 shows the weight loss analysis, differential heat flow, and the weight loss rate of free-standing MD and MCD thin films as a function of temperature in the range of 30 °C–600 °C. Based on the data in figures 8(a), (b), the sample weight loss during heating (known as TGA) may be divided into three regions. Weight losses of ~18.5, ~29, and ~8.8% were measured in the T ranges of 30–220, 220–325, and 325 °C–600 °C, respectively. Major reasons for weight losses in the low, middle (maximum loss region), and high T regions may be due to surface moisture evaporation, DNA (CTMA-DNA) decomposition, and evaporation of single-stranded DNA, respectively. We calculate the derivative thermogravimetry (DTG) (weight loss rate defined by dm/dt) of free-standing MD and MCD thin films with various [MNP] (figure S1, OSD). The amount of weight lost at low T (e.g., 75 °C) decreased with increasing [MNP] in the low T region. But weight loss rate increased up to a certain [MNP] (e.g., 10 mg of MNPs in an MD thin film at 230 °C) followed by a reduction in the rate with further increase in [MNP] in the middle T region. The trends agreed well with the TGA measurements.

Figures 8(c), (d) show the DTA curve demonstrating the heat flow change as a function of T in a nitrogen gas chamber. For MD thin film, an endothermic (heat absorbed by the sample) peak was observed at ~90 °C, and two exothermic (heat released by the sample) peaks were noted at ~230 °C and ~320 °C. Similarly, for MCD thin film, two endothermic peaks at ~80 °C and ~240 °C and an exothermic peak at ~300 °C were observed. The heat absorbed and released by the thin film during the flow of the gas was influenced by DNA decomposition and different solvents.

The weight loss from MD and MCD thin films with varied [MNP] in three different temperature regions (i.e., 30 °C–220 °C, 220 °C–325 °C, and 325 °C–600 °C) are discussed in figures 8(e), (f). Roughly, weight lost from MD and MCD decreases with increasing [MNP]. Figures 8(g), (h) show endothermic and exothermic reactions at three characteristic temperatures of MD and MCD thin films as obtained by DTA. A monotonic decrease of heat flow with

increasing [MNP] for MD thin films (measured at ~230 °C) was observed. In contrast, the V-shape trend of heat flow for MCD thin films (at ~240 °C) was observed. Variations in weight loss and differential thermal analysis controlled by T result from physical and chemical changes [45–49].

4. Conclusions

We have developed fabrication methodology for DNA (dissolved in water) and CTMA-DNA (dissolved in 1-butanol) thin films of various concentrations of [MNP] and discussed significances of optical (UV–vis absorption, refractive index and extinction coefficient, Raman spectra, cathodoluminescence (CL)), magnetic (magnetic field-dependent (M–H) and temperature-dependent (M–T) magnetizations), and thermal properties (TGA, DTG, and DTA). MNP-embedded DNA and CTMA-DNA thin films showed increasing UV–vis absorption and increasing n and k with increased [MNP]. By contrast, Raman and CL spectra showed suppressed signals with increasing [MNP]. In addition, M–H and M–T in field cooling and zero field cooling modes were conducted to understand the magnetic behavior of MNPs in DNA and CTMA-DNA thin films. The M increased monotonically with increasing [MNP] and reached the saturation magnetization (M_S). Due to the magnetic characteristics of MNPs, MNP-embedded DNA and CTMA-DNA thin films revealed the dominant superparamagnetic behavior. Finally, we conducted TGA, DTG, and DTA measurements for understanding the thermal stability and decomposition of free-standing DNA (CTMA-DNA) thin films with various [MNP]. These characterizations may be useful in various research fields such as optoelectronics (data storage, data reading, and photo-detectors) and biomedicine (magneto resonance image, drug delivery, chemotherapy, and hyperthermia therapy).

ORCID iDs

Mallikarjuna Reddy Kesama ⓘ https://orcid.org/0000-0003-1708-5605
Sreekantha Reddy Dugasani ⓘ https://orcid.org/0000-0001-5805-8713
Sung Ha Park ⓘ https://orcid.org/0000-0002-0256-3363

References

[1] Steckl A J 2007 Nat. Photon. **1** 3–5
[2] Grykien R et al 2014 Opt. Mater. **36** 1027–33

[3] Chen I, Chiu Y W and Hung Y C 2012 *Japan. J. Appl. Phys.* **51** 031601

[4] Yumusak C, Singh T B, Sariciftci N S and Grote J G 2010 *Appl. Phys. Lett.* **95** 263304

[5] Lai S, Barbaro M and Bonfiglio A 2015 *Appl. Phys. Lett.* **107** 103301

[6] Kesama M R *et al* 2016 *ACS Appl. Mater. Interfaces* **8** 14109–17

[7] Chopade P *et al* 2017 *Nanotechnology* **28** 405702

[8] Niemirowicz K, Wilczewska A Z and Car H 2013 *CHEMIK* **67** 836–41

[9] Koul S and Hakim N U D 2018 *Trans. Electr. Electron. Mater.* **19** 1–11

[10] Kesama M R *et al* 2018 *Colloids Surf.* B **167** 197–205

[11] Moreira E, Fraga L A, Mendonca M H and Monteiro O C 2012 *J. Nanopart. Res.* **14** 937

[12] Gnapareddy B *et al* 2015 *Sci. Rep* **5** 12722

[13] Ajroudi L *et al* 2010 *J. Cryst. Growth* **312** 2465–71

[14] Chesnel K *et al* 2014 *J. Phys.: Conf. Ser.* **521** 012004

[15] Meerod S, Tumcharern G, Wichai U and Rutnakornpituk M 2008 *Polymer* **49** 3950–6

[16] Heckman E M *et al* 2005 *Appl. Phys. Lett.* **87** 211115

[17] Ouchen F *et al* 2012 *Appl. Phys. Lett.* **101** 153702

[18] Lee N *et al* 2015 *Chem. Rev.* **115** 10637–89

[19] Ekariyani N Y *et al* 2016 *AIP Conf. Proc.* **1755** 150016

[20] Pershina A G, Sazonov A E and Filimonov V D 2014 *Russ. Chem. Rev.* **83** 299

[21] Pankhurst Q A, Connolly J, Jones S K and Dobson J 2003 *J. Phys. D: Appl. Phys.* **36** R167

[22] Jacek N 2014 *J. Appl. Phys.* **116** 234701

[23] Arasu V *et al* 2017 *Sci. Rep.* **7** 11567

[24] Kouassi G K and Irudayaraj J 2006 *Anal. Chem.* **78** 3234–41

[25] Li X *et al* 2012 *J. Magn. Magn. Mater.* **324** 1410–8

[26] Ghaemi M and Absalan G 2014 *Mikrochim. Acta.* **181** 45–53

[27] Inagaki T, Hamm R N, Arakawa E T and Painter L R 1974 *J. Chem. Phys.* **61** 4246–50

[28] Samoc A, Miniewicz A, Samoc M and Grote J G 2007 *J. Appl. Polym. Sci.* **105** 236–45

[29] Hebda E *et al* 2012 *Mol. Cryst. Liq. Cryst.* **556** 309–16

[30] Lee G J, Kwon Y W, Kim Y H and Choi E H 2013 *Appl. Phys. Lett.* **102** 021911

[31] Ban G *et al* 2009 *Nanoscale Res. Lett.* **4** 321–6

[32] Lee N, Schuck P J, Nico P S and Gilbert B 2015 *J. Phys. Chem. Lett.* **6** 970–4

[33] Shen H 2003 *Chin. Sci. Bull.* **48** 2698

[34] Kundu S *et al* 2017 *J. Mater. Chem.* C **5** 2577–90

[35] Zhu Y *et al* 2012 *Lumin* **27** 74–9

[36] Lee U R *et al* 2009 *J. Polym. Sci.* A **47** 5416–25

[37] Weizmann Y, Patolsky F, Katz E and Willner I 2003 *J. Am. Chem. Soc.* **125** 3452–4

[38] Pershina A G, Sazonov A E and Filimonov V D 2014 *Russ. Chem. Rev.* **83** 299

[39] Nakamae S 2005 *Phys. Rev. Lett.* **94** 248102

[40] Mizoguchi K and Sakamoto H 2015 *Crystals* **5** 475

[41] Dugasani S R *et al* 2013 *Sci. Rep.* **3** 1819

[42] Robinson I *et al* 2010 *Nanoscale* **2** 2624–30

[43] Kwon Y W *et al* 2012 *Sci. China: Chem.* **55** 814–21

[44] Dutta P *et al* 2006 *J. Appl. Phys.* **99** 08H105

[45] Hebda E, Niziol J, Pielichowski J, Sniechowski M and Jancia M 2011 *Chem. Chem. Technol.* **5** 397–402

[46] Jacek N *et al* 2016 *Opt. Mater.* **56** 84–9

[47] Zhou Y 2017 *Sci. Rep.* **7** 41741

[48] Shen L, Laibinis P E and Hatton T A 1999 *Langmuir* **15** 447–53

[49] Jacek N *et al* 2017 *J. Mater. Sci.: Mater. Electron.* **28** 259–68